Effect of shear on Rayleigh-Taylor mixing at small Atwood number

Bhanesh Akula, Malcolm J. Andrews, and Devesh Ranjan

Effect of shear on RT mixing at small Atwood number

Authors

Bhanesh Akula

Texas A&M University, Department of Mechanical Engineering, 3123 TAMU, Texas 77843-3123, USA

Malcolm Andrews

Los Alamos National Laboratory, Los Alamos, NM 87545, USA

Devesh Ranjan*

Texas A&M University, Department of Mechanical Engineering, 3123 TAMU, Texas 77843-3123, USA

979-845-3580 (Tel)

979-845-3081 (Fax)
*Corresponding Author: dranjan@tamu.edu

Abstract

The effect of shear on the development of Rayleigh-Taylor instability is studied at an Atwood number of 0.035 using the gas tunnel at Texas A&M University. Two types of diagnostics, imaging and simultaneous hot wire and cold wire anemometry are used to measure mix widths, point wise instantaneous velocities, and density. Image analysis has shown that the superposition of shear on Rayleigh-Taylor instability development increases the mixing width and growth rate at early times $(\tau = \dfrac{x}{U}\sqrt{\dfrac{A_t g}{H}} \ll 1)$. In particular, the mixing region shows distinct characteristics of shear (Kelvin-Helmholtz instability) and buoyancy (Rayleigh-Taylor instability). The Kelvin-Helmholtz instability is observed to be dominant at early times, and the Rayleigh-Taylor instability at late time ($\tau > 1$). In the late-time self-similar regime ($\tau > 1$), the mix width growth rate coefficient obtained using digital image analysis converge to a value between 0.06-0.07 for the compound buoyancy and shear (KH+RT) driven flows. Vertical velocity fluctuation rms values at the mixing layer centerline are measured using a hotwire technique. These rms values are correlated to the centerline mixing width growth rate, and this growth rate coefficient is found to lie between 0.06-0.07 at $\tau > 1$ for the KH+RT flows. The transition in flow dominance from shear instability to Rayleigh-Taylor instability is observed to correspond with Richardson numbers $(Ri = \dfrac{-2hg\Delta\rho}{\rho\Delta U^2})$ of -1.5 to -2.5. Molecular mixing between the fluids is examined by looking at the probability density function distribution of the density fluctuations. A different type of mixing behavior is observed over time for the compound cases compared with the transient development of Rayleigh-Taylor driven mixing.

I. INTRODUCTION

Coupled buoyancy and shear driven mixing occurs in various natural and technological environments such as in the atmosphere and oceans [1], mixing in combustion chambers, chemical reactors [2], discharges into rivers [3], and Inertial Confinement Fusion (ICF) fuel capsules [4]. The problem of shear with unstable stratification is not well studied compared with the buoyancy stabilizing shear case, and limited experimental data is available in the literature for the shear with unstable stratification case. This paper presents results from an experimental study on compound buoyancy and shear flows. For the present compound buoyancy and shear dominated flows, the mixing process starts through a shear dominated phase with linear mix width growth, and ends with buoyancy dominated mixing with quadratic mix width growth.

The Rayleigh-Taylor instability occurs whenever the interface between two fluids of different densities is accelerated in a direction such that $\nabla p \bullet \nabla \rho < 0$, where p is pressure and ρ is fluid density [5]. One important parameter that characterizes RTI is the Atwood number (A_t) defined by equation (1), where ρ_1 is the heavier fluid density and ρ_2 is the lighter fluid density. Atwood number is a non-dimensional measure of the density difference between the two fluids.

(1) $\qquad A_t = \dfrac{\rho_1 - \rho_2}{\rho_1 + \rho_2}$

Mikaelian [6] studied combined Richtmyer-Meshkov/Rayleigh-Taylor (RMI/RTI) and Kelvin-Helmholtz instability (KHI) analytically for incompressible fluids at early mix development times. Mikaelian [6] and Hoffmann [7] also emphasized the presence of this combined instability in an ICF fuel capsule when the incidental shock/blast wave is oblique to the interface due to the asymmetry in the drive. Mikaelian [6] noted that the effect of KHI is more pronounced in the combined instability at the fuel-ablator interface where the Atwood number (~ 0.8) is less compared with the fuel-DT gas interface (A_t ~1.0). It was shown that in the linear regime (at early times), for typical ICF parameters, the longer wavelength perturbations are stabilized by constant acceleration behind the shock wave. Mikaelian [6] also pointed out that the interplay between KHI, RTI and RMI is complicated as each have different wave number dependencies. Recent simulations by Thomas and Kares [8] have confirmed that the drive asymmetry can lead to penetration of ablative material into the central hotspot, and the turbulence generated by the instability of these penetrated structures will cause fuel dilution and eventual ignition failure.

Classically, small perturbations at the RTI interface grow in size with time and begin interacting with one another, which leads to turbulent mixing between the two fluids. Youngs [9] divided the growth of these perturbations into three regimes. The first regime is a linear growth regime where perturbations grow exponentially according to linear stability theory [10]. Linear stability theory is valid for small times after the onset of the instability, and predicts that smaller wavelength perturbations grow exponentially faster than longer wavelengths for RTI. The second regime describes the growth of small wavelength perturbations becoming saturated when the amplitude of the perturbations becomes close to half of their wavelength. This saturation was demonstrated experimentally by Lewis [11]. In this regime, the exponential growth of successively longer wavelength perturbations persists and eventually the flow is dominated by longer wavelengths; however, if longer wavelengths are absent in the initial perturbations,

then nonlinear interactions between saturated smaller wavelengths structures (mode coupling) lead to larger structures. In the third regime, memory of the initial conditions is lost and the two-fluid mix will reach self-similar growth. The three regime explanation of Youngs [9] is based on observations from experiments by Read [12], Lewis [11], numerical simulations, and turbulent plane mixing layer theory. Although Youngs used plane mixing layer theory as inspiration for his theory, the RTI mixing layer has shown a broad range of values for the growth rate coefficient, that vary for different experimental setups based on the initial conditions at the splitter plate [13, 14]. The three regime phenomenology has been challenged in recent years, with recognition that the fully self-similar development may not occur in an experiment due to the presence of initial long wavelengths that cause an acceleration of the mix layer development [15] which, in turn, causes "bubble competition" and a variable growth rate coefficient.

In contrast to the RTI phenomenology, the KHI occurs when two fluids of different velocities interact. In KHI, like RTI, the mixing between the two streams also leads to turbulence. KHI between two parallel streams is more usually referred to as the plane mixing layer problem. Goertler [16] obtained the first analytical solution to the mixing layer problem with two streams. He assumed that eddy viscosity is constant across the mixing layer and obtained a series solution for the velocity distribution. A summation of the first two terms in this solution, and neglecting all other terms, is considered by many researchers to be accurate enough for all practical purposes. Using a similar approach, Sabin [17] derived a first order approximate solution with a pressure gradient for the plane mixing layer problem that compared well with the zero pressure gradient solution of Goertler [16] at lower velocity ratios. He suggested the use of the same eddy viscosity for all pressure gradients from his experimental work, and he quantified the dependence of mixing layer spreading rate on the velocity ratio (velocity of slow moving stream/velocity of fast moving stream) between the two streams.

Leipmann and Laufer [18] made the first measurements of the turbulence inside a mixing layer of an air stream coming out of a nozzle into quiescent surroundings. They estimated the spreading rate and asymmetry of the mixing layer, and compared these estimates with available theories and experiments. They showed that phenomenological theories, like the Prandtl mixing layer theory, are only reasonable when predicting the mean velocity variations, and they fail to predict higher order turbulent quantities. Yule [19] reviewed plane mixing layer theory and the experimental data available up to 1972. He conducted mixing layer experiments in a two-stream wind tunnel at different velocity ratios. Yule compared the two stream mixing layer experiments with a free mixing layer (absence of second stream), and observed that the large eddy structure is affected by the presence of the second stream. Yule also pointed out that Goertler's solution did not consider the asymmetry of the mixing layer, and suggested a method to calculate this asymmetry. Bell and Mehta [13] studied the effect of initial conditions in plane mixing layer at a velocity ratio of 0.6. They observed a 20% difference in mixing growth rate coefficient between tripped and untripped initial conditions.

In the case of KHI, small perturbations at the interface grow in size with time and form into spanwise vortical rollups. Winant and Browand [20] studied the process of vortex pairing between two neighboring spanwise vortices using flow visualization, and they observed that pairing does not always start at the same spatial location due to small spatial and temporal irregularities in vortical structures. They also proposed a model for mixing width growth rate based on earlier non-interacting vortex theories. Browand and Weidman [21] used a conditional sampling technique to study different stages of vortex pairing at small Reynolds numbers (defined based upon mixing width, velocity difference, and kinematic

viscosity). The first stage was just after the pairing process, and the second stage was during the pairing process. They measured higher values of turbulent Reynolds stress production during the pairing process. They noted a similar pairing mechanism as observed by Brown and Roshko [22], and proposed that the pairing mechanism at lower Reynolds numbers was universal and can be extended to higher Reynolds numbers. At Reynolds numbers around 2500 Koochesfahani and Dimotakis [23] observed a large amount of high velocity stream fluid trapped inside the rollup with very little or no mixing with the other stream. As the Reynolds number increased above 23000, beyond the "mixing transition," they observed improved mixing between the streams due to the three dimensionality of the flow, with a still higher amount of high velocity stream fluid at the center of the mixing layer. Lasheras and Choi [24] studied the formation of counter rotating streamwise vortices on the braids of two dimensional spanwise vortex tubes for different types of perturbations at the splitter plate. Their investigation centered on the growth of these streamwise vortices and the coupling process with the two-dimensional span wise vortices that make the flow three-dimensional. They observed the same coupling process for both the horizontal and vertical initial perturbations. Brown and Roshko [22] studied the effect of density difference (without any acceleration at the interface, i.e., without any stable or unstable stratification) on flow structure in plane mixing layers. They studied the large-scale structure for density ratios (density of low velocity stream/density of high velocity stream) of 0.14, 1.0, and 7.0. They noticed similar structures at all density ratios and the change in the value of spreading angle, which correlates to the mixing width growth rate, was relatively small compared to the change in the density ratios.

It is important to study the effect of KHI in a stratified flow because it affects most of the mixing processes in the atmosphere and ocean flows [1]. The relative strength of buoyancy to shear can be quantified using the Richardson number (Ri), defined by equation (2) where g is gravity, $\Delta\rho$ and ΔU are the density and velocity differences, respectively, ρ and $2h$ are the measured mean density and the mixing width. The Richardson number, defined based on the initial mixing width at the onset of the instability, is referred to here as initial Richardson number. The Richardson number values are positive for stably stratified flows and negative for unstably stratified flows.

$$(2) \qquad Ri = \frac{-g\left(\frac{\partial \rho}{\partial z}\right)}{\rho\left(\frac{\partial u}{\partial z}\right)^2} = \frac{-2hg\Delta\rho}{\rho(\Delta U)^2} = \frac{-4ghA_t}{(\Delta U)^2}$$

Thorpe [25] studied stably stratified shear flow by filling a long rectangular tube with different fluids and then tilted, the tube before bringing it back to the horizontal position, in order for the instability to develop. From different experiments, by varying the parameters defining the Richardson number, Thorpe [26, 27] observed that at a Richardson number value of 0.33 striations started to appear, and the turbulence started to decay. He observed that the ratio of the velocity interface thickness to the density interface thickness (velocity and density interface thicknesses are defined as the distance between the points in the mixing layer where the velocity and density reach their respective free stream values) increases with increased values of the initial Richardson number. The final Richardson number, defined at the center of the layer based on both velocity and density interface thickness, remained constant irrespective of the initial Richardson number after a fixed non-dimensional time from the onset of turbulence. Browand and Winant [28] performed experiments in a stratified shear layer and noticed that the mixing layer width collapsed onto a single final curve irrespective of the initial density difference

between the streams. They concluded that turbulence due to shear cannot be maintained in a stably stratified fluid. Koop and Browand [29] studied the turbulence and flow structure at different Richardson numbers in a stably stratified fluid with shear. They observed that at low Richardson numbers < 0.15, the vortical structures similar to the plane mixing layer still persist in their visualization experiments, which is similar to Thorpe's observation [26]. The flow induced by these vortical structures moved the heavier fluid to the top and the lighter fluid to the bottom. The vortical structures grew in size due to vortex pairing, but they were unable to work against buoyancy and broke down before re-laminarizing into a non-turbulent flow. As the initial Richardson number increased further, the formation of the vortices was not observed and the flow structure was replaced by interfacial waves. Koop and Browand showed that the decay of turbulence in the re-laminarizing region is similar to grid turbulence decay. They compared the value of the maximum Richardson number at which turbulence started to decay with the non-interacting vortex model, and found good agreement with Thorpe's experiments [26]. They also observed a decreased amount of molecular mixing with increasing values of initial Richardson number at a point well after the start of turbulence decay.

Shifting our attention to unstably stratified flows, Shumlak and Roderick [30] observed stabilization of RT instability with shear in Z-pinch implosions from their analytical and numerical work, including the effect of magnetic forces. Lawrence *et al*. [26] performed a stability analysis, with and without a finite interface thickness, for KH+RT flows. They also performed experiments in an unstable configuration in a water channel and noticed the transformation from shear instability dominated flow to RTI dominated flow. They presented the flow structure evolution in the channel for a compound shear and buoyancy case. Snider and Andrews [31, 32] studied the effect of shear on RTI experimentally at small Atwood number (<0.005). They did not notice any change in mixing width compared with RTI at late times in their compound shear and buoyancy experiments. They also observed a similar flow structure evolution as Lawrence *et al*. [33]. Due to experimental setup limitations Snider and Andrews [31, 32] could not achieve a higher velocity difference between the two streams. Snider and Andrews [34] simulated the compound case using a $k - \varepsilon$ model, and found that the addition of shear to RTI decreased the mixing width growth rate, countering the perception that the addition of instabilities would increase the growth rate. Snider and Andrews [31, 32, 34] concluded that the addition of shear to unstable buoyancy would not increase the mixing width growth rate, and more experiments were needed to check their simulations. More recently, Olson *et al*. [35] studied the effect of shear on RT instability numerically in the non-linear regime, immediately after the linear regime, and found that the peak mixing width growth rate (highest mixing growth rate observed in time) changed non-monotonically with the increased amount of shear. They found an optimum value of shear for fixed RTI parameters at which the peak mixing width growth rate is minimum. The flow structure resembled pure KH instability at the point of lowest growth rate. They observed that the addition of a small amount of shear decreased the amount of vertical turbulent kinetic energy, channeled from the available energy, and caused smaller mixing width growth rate.

Here we study the effect of shear on RTI mixing widths and its embedded structures. Linear stability theory indicates that any addition of shear will increase the growth rates at earlier times [10], and it would be useful to know whether the same effect is observed at later times. In the present scenario, RTI combined with KHI is studied using the Texas A&M gas tunnel facility at an Atwood number of 0.035. Flow structures observed due to RTI, KHI, and KH+RT are compared with each other at this Atwood number. Different KH+RT cases are compared with each other in terms of mixing width, and their mixing

width growth rate, at the same Atwood number, by changing the convective velocity of one of the streams. The experimental setup used for this study is described in Section 2. Section 3 describes the flow visualization technique used for measuring mixing width, as well as the simultaneous 3 wire and cold wire anemometry technique used for measuring instantaneous velocity and density. The results obtained from both diagnostics are discussed in Section 4.

II. Experimental Setup

A wind-tunnel type facility was built at Texas A&M University to study buoyancy driven mixing. The facility is capable of producing the RTI at Atwood numbers up to 0.75 with and without shear. A schematic of the facility is shown in Figure 1. This is a statistically steady system capable of collecting data for long periods of time. The facility consists of two 0.6m by 0.6m flow sections separated by a splitter plate (Figure 1, side view). Each section is fitted with flow straighteners and wire mesh screens to make the flow uniform throughout the cross section and reduce its turbulence level. Air, supplied from one of the air blowers, flows into the top section. The bottom section is supplied with an air and helium mixture. Helium is introduced (at a rate of approximately 0.0066 lbm/s to give an Atwood number of 0.035) into the connection between the bottom stream air blower and the channel. The mixture passes through a series of baffles to ensure uniform mixing between both gas streams. The 2m long test section starts after the splitter plate where the mixing between the two streams starts. Further details about the components and detailed design considerations for the facility are given by Banerjee and Andrews [36].
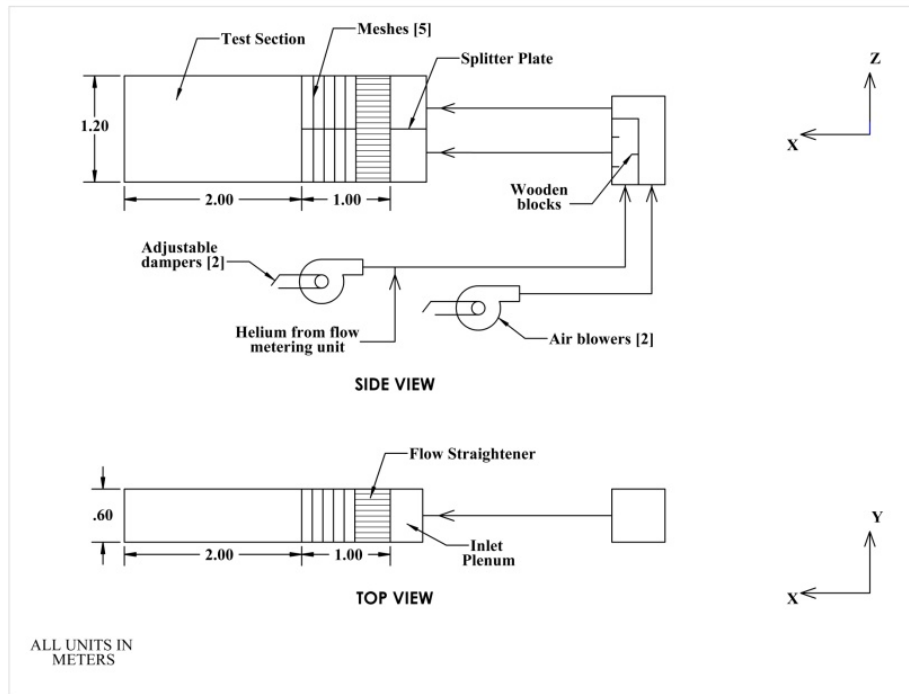
Figure 1: Schematic of the experimental setup of the gas tunnel facility at Texas A&M.

This facility is a convective type RTI system as opposed to the classic closed box type system (where two fluids are placed in an unstable configuration without any mean velocity) used by earlier RTI researchers [10-12]. The facility is similar to the water tunnel facility at Texas A&M, where very small

Atwood number (less than 0.001) RTIs have been studied using both warm and cold water as working fluids [32, 37]. In the current facility, the time t after the onset of instability is calculated using Taylor's hypothesis [38], $t = x/U$, where x is the distance from the splitter plate and U is the average of the convective velocities of both the streams. For RTI experiments, U is kept the same for both streams to eliminate the effect of shear on the instability. In the present work, shear is superimposed intentionally on the density difference across the streams to study the effect of shear on RTI.

Helium is introduced into the bottom stream of the channel from a helium metering system. For a particular experiment, a constant volumetric/mass flow rate of helium is maintained by choking helium from pressurized gas cylinders (at 2100 psi) with a small orifice plate and pressure regulators. Varying the orifice size of the orifice plate changes the mass flow rate of the helium. Gas cylinders are replaced once the pressure drops below 500 psi, as the orifice plate does not choke the helium below this pressure. Details about the calibration procedure for the orifice plate and related theoretical background are given by Banerjee and Andrews [36].In order to study the effect of shear on RTI at a particular Atwood number only the top stream velocity is varied in the experimental facility. Bottom stream velocity and density are related by equation (3), in which A is the cross section area of the bottom stream, ρ_{air}, and ρ_{he} are density of helium and air respectively. Adjusting the bottom stream velocity U_b changes the bottom stream density ρ_{bottom}^{mix} (thus Atwood number) for a fixed helium flow rate $\dot{m}_{he}$. To maintain the same Atwood number $\dot{m}_{he}$ needs to be adjusted in accordance with U_b, if the bottom stream velocity is changed. As only certain sizes of orifice plates are available, the choice of U_b becomes less flexible. Thus only top stream velocity is changed for the present work and U_b is kept constant for all the cases.

$$(3) \qquad \rho_{bottom}^{mix} = \rho_{air} + \frac{\dot{m}_{he}}{U_b A} \left[1 - \frac{\rho_{air}}{\rho_{he}} \right]$$

III. Diagnostics

Two types of diagnostics are used in this study to obtain qualitative and quantitative information about the developing flow fields, namely visualization and hot wire anemometry. Visualization results are discussed thoroughly in this paper, as well as a sample of the results obtained from hot wire anemometry. Both of these techniques were used by previous researchers working with this facility to study the RTI at different Atwood numbers [38, 39]. These techniques are briefly explained here; however, readers are encouraged to examine references [36, 38, 40], which provide an in-depth analysis of these techniques. The results presented here correspond to an Atwood number of 0.035±0.0015.

For flow visualization, the channel is backlit using 35 fluorescent lights behind diffusive Acetate paper sheets. Fog particles, composed of condensed ethylene glycol droplets (ATMOSPHERES fog fluid, High End Systems), are injected into one of the streams. The addition of fog to the stream changes the Atwood number by 2-2.5% at the Atwood number studied in this paper. After injecting the fog particles, images are taken at a rate of 60 images per minute, for up to four minutes.

Images are taken using a Nikon D-90 DSLR camera at a 35mm focal length, 100 ISO, F11 aperture and 1/160 shutter speed. Beer-Lambert's law, given by equation (4), indicates the relationship

between the intensity of light I_0 from a source and I_m, the intensity of same light after travelling through a medium of optical thickness λ. Optical thickness λ is the product of the light extinction coefficient of the medium (κ), thickness of the medium (s), and the density of the medium (ρ). For a medium with constant light extinction coefficient, λ is only dependent upon ρs. For an optically thin medium ($\lambda \ll 1$), the ratio I_m / I_0 is directly proportional to λ and the measured intensity I_m can be used to estimate ρs through a linear relationship[41]. Calibration is performed inside the tunnel using a wedge shaped block filled with fog particles and air (constant ρ) with the same camera settings as the experiment. The wedge's cross-section decreases along the edge, and consequently so does the thickness of the light extinction medium (s), increasing the measured intensity I_m. When I_m / I_0 ratio values are plotted against the distance along the edge, the ratio varies linearly on the brighter side of the wedge [36]. This calibration determines the fog concentration to be used for the experiments so that the light intensity ratio I_m / I_0 values obtained from the images are directly proportional to the fluid volume fraction satisfying the optically thin medium approximation.

(4) $\qquad I_m = I_0 e^{-\kappa p s} = I_0 e^{-\lambda} \approx I_0 (1 - \lambda)$

The images taken during the experiment are ensemble averaged, and the ensemble averaged intensities obtained are corrected for non-uniform background using the formula presented in equation (5), where $I_{corr} (= I_0^{uniform}(1-\lambda))$ is the corrected intensity, $I_0^{uniform}$ is the uniform background intensity value to which the intensities have to be corrected, I_m is the measured intensities from the ensemble averaged image, and I_0 is the actual background intensity value. See Banerjee and Andrews [36] for further details about wedge calibration and background correction. Volume fraction contours are obtained from these corrected intensity values.

(5) $\qquad I_{corr} = \dfrac{I_0^{uniform}}{I_0} I_m$

Simultaneous 3 wire and cold wire anemometry (S3WCA) is used to simultaneously pointwise measure velocities and density. This technique was developed by Kraft $et~al.$ [40] based on earlier work on simultaneous measurements of temperature and velocities by Hishida $et~al.$ [42] and Vukoslavčević $et~al.$ [43]. Temperature is used as a marker for density by gently heating one of the streams. The difference between the temperature measured in the mixing layer and the free stream temperature of the streams can be directly correlated to the volume fraction of the streams as the Lewis number is close to 1 [38]. The stream is typically heated by 2°C at low Atwood numbers as a higher amount of heating causes larger uncertainties in Atwood number. A three-wire probe from Dantec Dynamics (model# 55P91) is used to measure the velocities at a point, and a cold wire probe is used to measure the temperatures. Both probes are placed side by side to measure temperature (density) and velocities simultaneously with a probe spatial resolution of 6 mm.

Calibration of the three-wire probe is performed at different volume fractions of air and helium before the experiment. For example, for an Atwood number of 0.1, the maximum volume fraction of

helium present in the channel would be 0.23. For this case, the calibration of the 3 wire probe is performed at helium volume fractions of 0.05, 0.1, 0.15, 0.2, and 0.25. A King's law (stated in equation (6), where E is the recorded voltage, A and B are King's law fit coefficients, U_{eff} is the velocity perpendicular to each wire, and n is power law coefficient taken as 0.5 for the present experiments) fit is made between the wire effective velocities (velocities converted into wire coordinates) and voltages from each wire. The coefficients for the King's law fit are calculated for each wire at each volume fraction.

(6) $\qquad E^2 = A + BU_{eff}^n$

   During the experiment, the temperature and wire voltages were recorded simultaneously at a frequency of 1000 Hz (limited by cold wire frequency) from the cold wire and the 3 wire probes, respectively. The temperature value recorded by the cold wire probe is converted into volume fraction using equations (7) and (8), which were developed from an energy balance [40]. In these equations, subscript 1 refers to top stream, subscript 2 refers to the bottom stream, $f_{m,i}$ is the mass fraction of stream i, $f_{v,i}$ is the volume fraction of stream i, c_p is the specific heat, T is the temperature, and ρ is the density.

(7) $\qquad f_{m,2}(t) = \left[1 + \dfrac{c_{p,2}}{c_{p,1}} \dfrac{T_2(t) - T_{mix}(t)}{T_{mix}(t) - T_1(t)} \right]^{-1}$

(8) $\qquad f_{v,2}(t) = \dfrac{\rho_1}{\rho_1 - \rho_2 + \dfrac{\rho_2}{f_{m,2}(t)}}$

   Further aspects of the technique, and the procedure to obtain velocities, is explained in detail by Kraft *et al.* [40].

IV. RESULTS

   The effect of shear on RTI is studied using the diagnostics described in the previous section to obtain the mixing width (defined as the distance between the 5% and 95% volume fraction contour at a particular stream wise location), and the instantaneous velocity and density data inside the mixing region. Experiments are performed at an Atwood number of approximately 0.035, with and without shear. The cases considered here are shown in Table I with uncertainties indicated in parenthesis.

Table I: Experimental cases considered for image analysis with uncertainties indicated in parenthesis.

Case name	Bottom stream velocity, m/s (U_2)	Top stream velocity , m/s (U_1)	$U_{average}$, m/s	$\dfrac{\rho_1 U_1 + \rho_2 U_2}{\rho_1 + \rho_2}$, m/s	Atwood Number	Max. Ri number	$\dfrac{U_1}{U_2}$
RT case	0.63	0.63 (0.02)	0.63	0.63	0.035 (0.003)		1.0
KH+RT 1	0.63	0.86 (0.02)	0.75	0.75	0.035 (0.003)	-6.9 (2.1)	1.4
KH+RT 2	0.63	1.03 (0.02)	0.83	0.84	0.035 (0.003)	-1.8 (0.4)	1.6
KH+RT 3	0.63	1.25 (0.02)	0.94	0.95	0.035 (0.003)	-0.8 (0.1)	1.9
KH	0.6	1.25(0.02)	0.93	0.93	0	0.0	2.1

In the definition of Richardson number given by equation (2) all the parameters are constant except the mixing width h; thus the variation of Ri along the tunnel is similar to the variation of mixing width. The Ri number becomes minimum (highest absolute value) at the end of the tunnel for the present experiments as shown in Table I.

A. Image Analysis Results

Flow visualization experiments are performed to evaluate the mixing width and its growth rate. An ensemble average of images is taken to evaluate the mixture fraction contours and mixing width. Figure 2 shows a sample bottom stream volume fraction contour set from an ensemble averaged image for the RT case from Table I. The volume fraction contours are discontinuous at various locations due to the method by which they are calculated, and non-uniformities present in the fog concentration far away from the mixing region. These discontinuities do not have any physical significance and are removed during image analysis by using a filter to remove all the points whose height difference is above 5cm (roughly 100 times the pixel resolution) than their adjacent point.
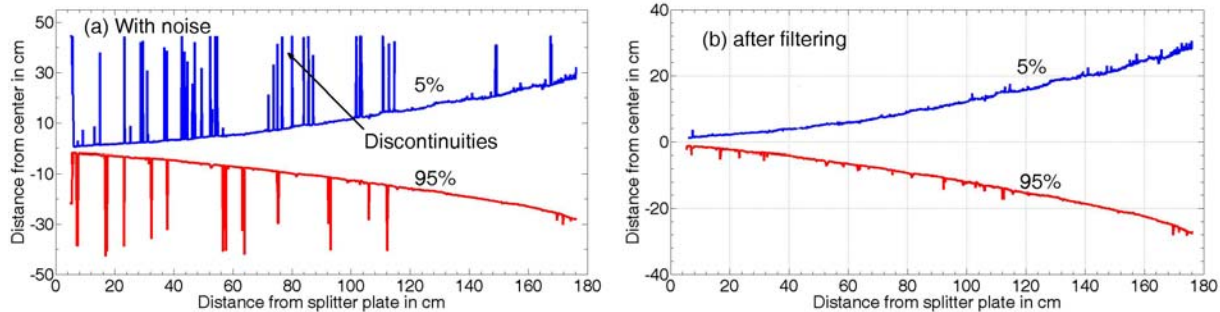
Figure 2: (Color online) Comparison of actual volume fraction contours to contours with discontinuities removed for RT case from Table I.

Figure 3 shows a comparison between the images taken with buoyancy only, with shear only, and with compound shear and buoyancy (top to bottom). Figure 3 also shows the associated volume fraction contours of the bottom fluid from ensemble averaged images for the same cases. The ensemble average uses over 200 images, taken at the rate of 60 images per minute. According to Banerjee and Andrews [36], this number of images is sufficient to obtain statistical convergence in density and mixing width measurements. For the buoyancy only case, vertical plumes characterize the flow. The buoyancy force at the interface causes shear between the rising lighter fluid and the falling heavier fluid, that forms the mushroom like structures in these vertical plumes. For the shear only case of Figure 3b, spanwise vortical structures are the main characteristic of the flow. These structures are large in number when closer to the splitter plate in the streamwise direction. The structures merge with each other to form larger structures with increased spacing downstream. These larger structures dominate the late time mixing, through bubble competition in RTI mixing, where larger structures tend to grow faster than smaller structures, which gives less space for smaller structures to grow and, in turn, shrinks them and inhibits the small structure growth [44]. For the compound shear and buoyancy case of Figure 3c, the flow is initially dominated by spanwise vortical structures formed due to the shear between the streams. Inspection of Figure 3c reveals that these vortical structures are stretched by buoyancy within the structures. Stretching of these vortical structures weakens the structures and the flow is eventually governed by buoyancy only

(see Figure 3c). This transition into buoyancy dominated flow structure is clearly observed for KH+RT 1, KH+RT 2 cases, but cannot be observed in the compound case KH+RT 3 as the shear between the streams is large enough to dominate buoyancy for a longer time. The KH+RT 3 case requires a longer test section beyond the length of the current test section for the flow to be governed by buoyancy only.
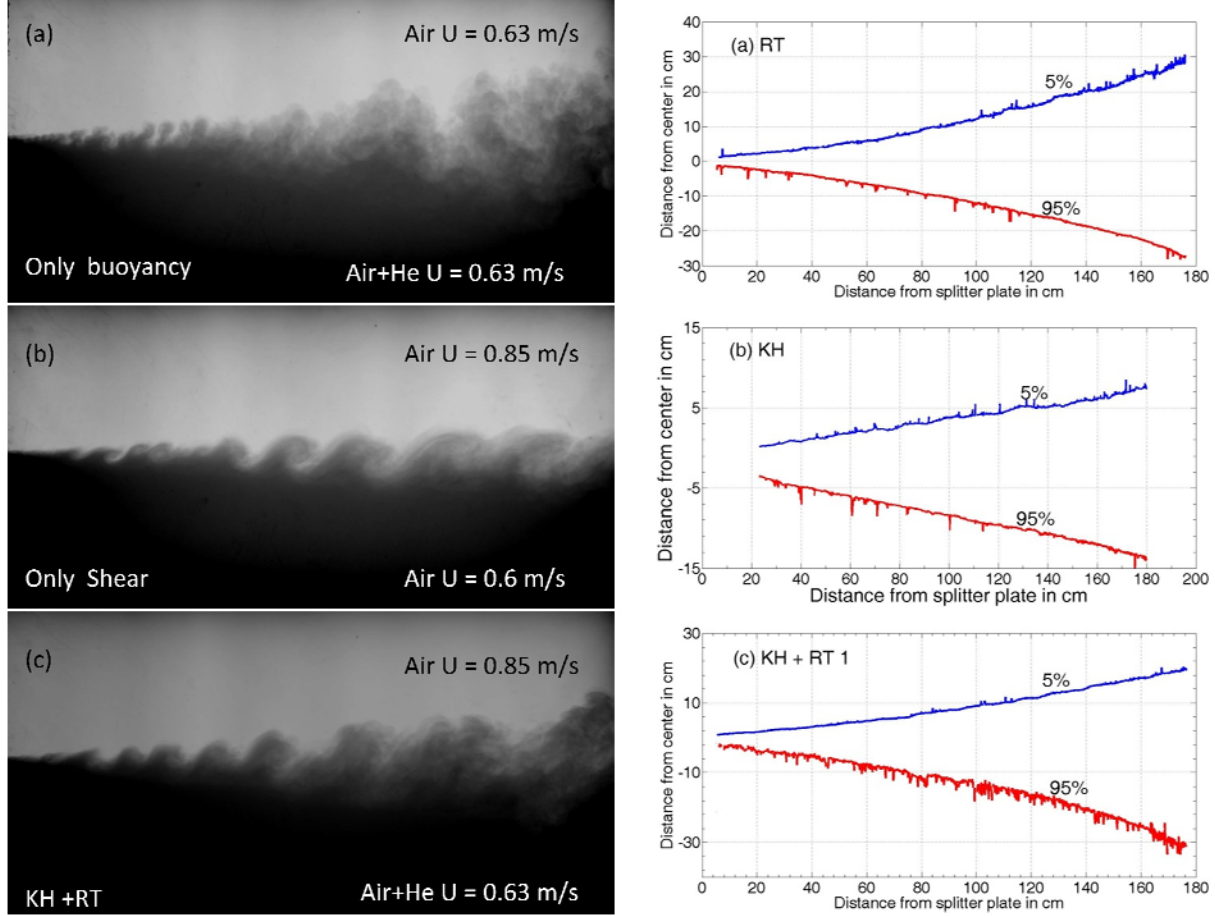

Figure 3: (Color online) Sample images taken for the flow with (a) only buoyancy, (b) only shear, and (c) combined buoyancy and shear at Atwood ~ 0.032 and corresponding volume fraction contours of bottom stream fluid $f_{v,2} = 0.05$ and $f_{v,2} = 0.95$ (Ensemble average of 200 images taken over 200 seconds).

Volume fraction contours obtained with flow visualization for the cases of Table I are shown in Figure 4. The case name is indicated on the top left corner for each plot. For each case the bottom stream volume fraction contours of 0.05 and 0.95 are plotted. The pure RT (top left) case shows a symmetric mixing layer with the highest mixing width at the end of the tunnel compared with the other cases (note the change of the vertical axis). The RT volume fraction contours are parabolic in shape indicating a

$A_t g \left(\dfrac{x}{U} \right)^2$ development of the self similar RTI mixing layers [9]. With an increase in shear (KH+RT 1-3), the mixing layer shifts toward the slower moving stream (bottom stream). This shift is higher for larger velocity differences, such as KH+RT 3, which shows larger asymmetry about the geometric

centerline compared with other cases (see Figure 4). This attribute is a typical characteristic of planar mixing layers [14].
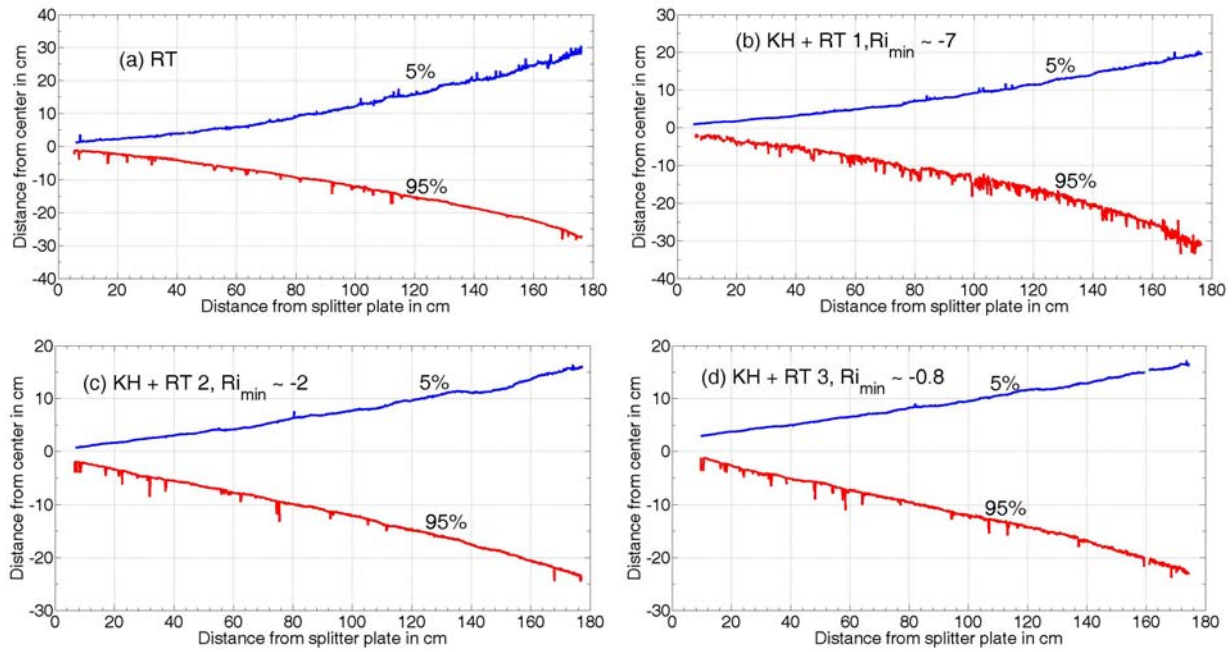
Figure 4: (Color online) Volume fraction contours of bottom stream fluid $f_{v,2} = 0.05$ and $f_{v,2} = 0.95$ for different shear cases: (a) no shear RT case, (b) KH+RT 1, (c) KH+RT 2, (d) KH+RT 3.
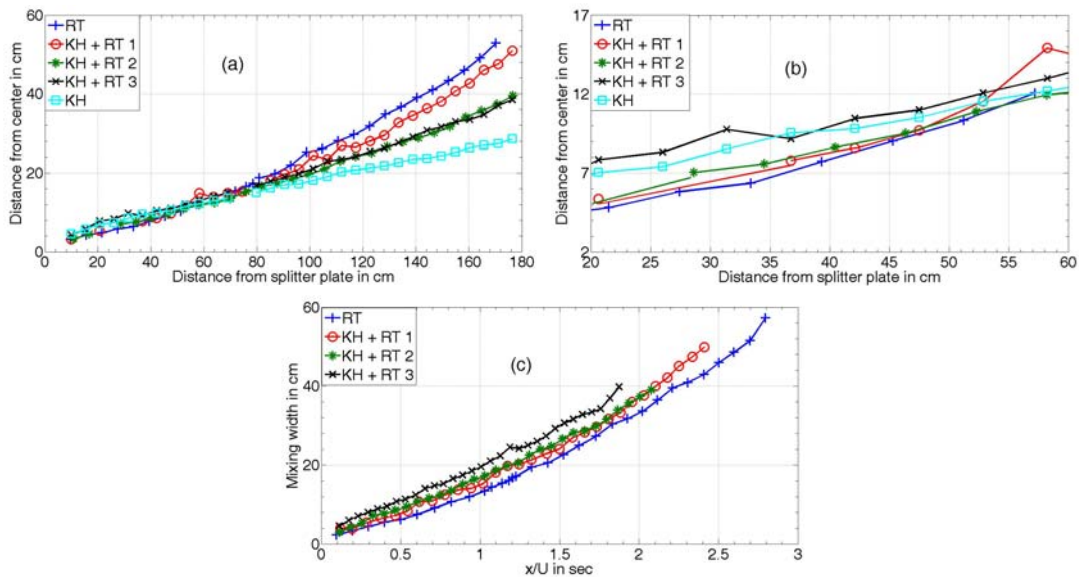
Figure 5: (Color online) (a) Mixing width variation for different KH+RT cases, (b) expanded view near the origin showing the variation closer to the splitter plate, and, (c) mixing width variation with time x/U.

Mixing width is defined as the distance between the 5% and 95% volume fraction contours of Figure 4, and is plotted in Figure 5 for all the cases of Table I. Visualization (Figure 3) shows that shear is predominant closer to the plate, and the flow is dominated by RT structures far away from the splitter plate for a compound case. Mixing width plots for compound cases KH+RT 1 and KH+RT 2 shown in Figure 4a also support this statement. They show linear variation closer to the plate, which represents the growth of a plane mixing layer growth and parabolic variation far away from the plate, representing the growth of a RTI mixing layer. The mixing width is larger everywhere for a compound case compared with the corresponding shear only case with the same ΔU value (see Figure 5a for KH+RT 3 vs KH or Figure 3b,c for KH+RT 1 vs KH1). This is due to the stretching of initial spanwise vortices closer to the plate and faster growing buoyancy structure far away from splitter plate. The expanded view near the origin (Figure 5b) shows the mixing width variation close to the splitter plate. The mixing width is greater closer to the splitter plate for the shear only case when compared with the RT case. This is due to the formation of spanwise vortical structures at the start of the instability. The KH+RT 3 case has a higher mixing width compared with the KH+RT 1, and KH+RT 2 cases close to the plate, as a larger amount of shear causes larger spanwise vortices that correspond to linear stability theory [5], which predicts that the initial growth rate is proportional to the square of the velocity difference between the streams. The mixing width variation for all five cases are curve fitted with a fourth order polynomial (defined by equation (9), where h, x are in cm) for numerical simulation comparison purposes. All five coefficients obtained for each case are shown in Table II. The coefficients shown here are valid only from $x = 10$ cm to 175cm, as the data available before $x = 10$ cm has larger uncertainties due to the small value of mixing width.

$$(9) \qquad h = \sum_{n=0}^{4} a_n x^n$$

Table II. Coefficients from curve fit for all the five cases calculated using equation (9)

|	a_0	a_1	a_2	a_3	a_4
RT	2.96	0.0135	0.003453	-2.00×10^{-5}	5.40×10^{-8}
KH+RT 1	2.51	0.1034	0.001698	-1.14×10^{-5}	4.08×10^{-8}
KH+RT 2	1.93	0.1468	0.000622	-4.90×10^{-6}	1.96×10^{-8}
KH+RT 3	3.04	0.1744	-5.63×10^{-5}	6.97×10^{-7}	2.56×10^{-9}
KH	2.97	0.1795	-4.37×10^{-4}	1.80×10^{-6}	-2.61×10^{-9}

The plane mixing layer problem (shear only case) is well studied [13, 20], and linear growth of these mixing layers in the self-similar regime is well known. The mixing growth rate coefficient for KHI flows is defined as $\dfrac{U_1 + U_2}{U_1 - U_2} \dfrac{dh}{dx}$. Youngs [9] proposed a parabolic growth of RTI mixing layers in the self-similar regime, and this description has been confirmed by numerous experiments and numerical simulations [15, 32]. The mixing growth rate coefficient for RTI flows, α, is defined by equation (10), using the expression for bubble mixing width h_b by Youngs [9], and a time/space conversion using Taylor's hypothesis for the present convective system.

(10) $h_b = \alpha A_t g t^2 = \alpha A_t g \left(\dfrac{x}{U} \right)^2$.

For the present small Atwood number RT experiments, the bubble mixing width h_b can be taken as half of the total mixing width [38]. This definition is extended to all the cases for the calculation of the mixing width growth rate coefficient α. For the cases with shear, the convective velocity is considered to be the density weighted average velocity of both the streams. At the present Atwood number of 0.035, the density weighted average velocity and the arithmetic average velocity are close (Table I). Kraft [39] used a linear fit between h_b and $A_t g t^2$ in the self-similar regime (at roughly 1-1.2m away from the splitter plate) to determine the growth rate coefficient α. Table III shows the growth rate coefficient values obtained from this method in column 2. No particular trend is currently observed for α using the linear fit method and the values are within the range of 0.074-0.094.

Table III: Comparison of growth rate coefficients α and β values for different cases using equation (10) and equation (11) with uncertainties indicated in parenthesis

Case	α from equation (10)	α from equation (11)	β
RT	0.074 (0.007)	0.074 (0.007)	--
KH+RT 1	0.094 (0.007)	0.066 (0.007)	0.21
KH+RT 2	0.083 (0.007)	0.050 (0.007)	0.17
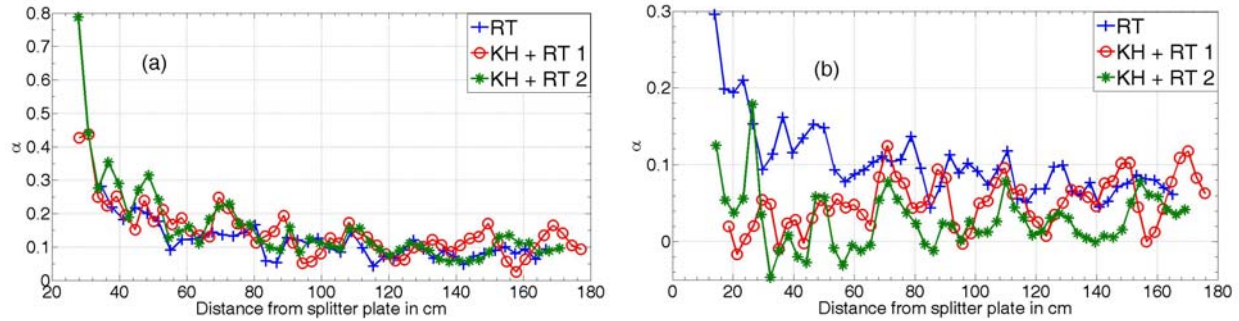
Figure 6: (Color online) Variation of growth rate coefficient α along the channel for different cases (a) using equation (10), (b) using equation (11).

Another linear fit method, similar to the one used by previous researchers (Banerjee *et al.* [38]), has been implemented to calculate the value of α. This method uses a moving window, in which a window of 100 pixels is moved down stream pixel by pixel. In this window, a fit is made between the half mixing width h_b and $A_t g t^2$, and the slope of the line is taken as α at the middle of the window. The mixing width growth rate variation along the channel for the 4 cases is shown in Figure 6a. In the RT self-similar regime, this method also finds a α value in the same range as the earlier method (see Table III). Closer to the splitter plate, the high shear case shows the highest value of α due to large spanwise vortices. Far away from the splitter plate and in the self-similar region, all the cases have α value within

the range of 0.073-0.094 (Figure 6). The way α is calculated for the KH+RT cases is reconsidered as gt^2 is not a proper scaling parameter for flows that have not yet reached the buoyancy-governed region. One way to consider the effect of shear in calculating α is proposed in equation (11), where β is the initial KHI growth rate. The α and β values, calculated using equation (11) by the moving window method, are plotted in Figure 6b, and the values observed at the end of the tunnel are tabulated in Table III. The value at the end of the tunnel is calculated by averaging the value of α obtained from the moving window averaging method in the last 40cm of the tunnel. The value of β for KH+RT cases is obtained from corresponding shear only case without buoyancy.

$$(11) \quad h_b = \beta \frac{\Delta U * x}{U} + \alpha A_t g \left(\frac{x}{U} \right)^2$$

The oscillatory behavior of α is caused by sudden changes in the mixing width gradient from ensemble averaging. Theoretically, this can be avoided by averaging a very large number of images. After the transition region, α calculated using equation (11) is closer to the RT self-similar value for the KH+RT 1 case. For the KH+RT 1 case, the average α value is close to zero before the transition region, where the flow is KHI dominated, and slowly increased to self-similar RTI value after the transition where the flow is RTI dominated. For the KH+RT 2 case, this transition is around 150 cm from the splitter plate and close to the channel exit. We conclude that the mixing layer may reach a self-similar value of RT case if more distance is available. Thus, calculating α from equation (11) tends to indicate more realistic values than just using $A_t g t^2$ as a scaling parameter when shear is involved.
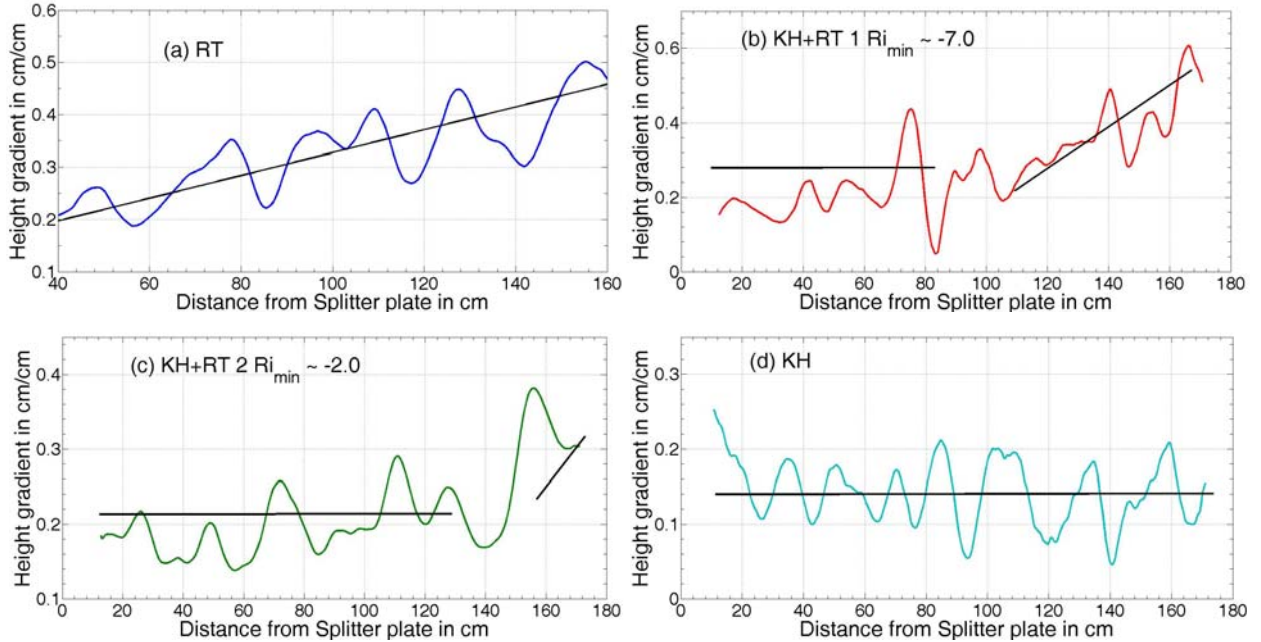
Figure 7: Mixing width gradient variation along the streamwise direction for (a) RT, (b) KH+RT 1, (c) KH+RT 2, and (d) KH cases. Black lines in each plot indicate the trend of mix width variation.

We now turn our attention to the transitional Richardson number. The Richardson number, defined by equation (2), quantifies the relative magnitudes of buoyancy compared with shear, and is well

known to be an important parameter for comparing various experiments with different operating conditions. The Richardson number value at which transition takes place from the shear driven flow to buoyancy driven flow can be obtained from the mixing width information. Here we determine the transition Richardson number by observing the trend of the mixing width gradient with downstream distance. The gradient is calculated by a moving window technique, in which two windows of 100 pixels in size (approximately two inches) are placed side-by-side and traversed downstream. Mixing width values are averaged in each window and the gradient is calculated using the averaged values. The gradient values obtained for the RT, KH+RT 1, KH+RT 2, and KH cases are plotted in Figure 7. The gradient variation shows oscillatory behavior due to small fluctuations in the mixing width information obtained from the image analysis.

Figure 7a shows a linear variation for the mixing width gradient confirming a parabolic growth of the mixing width for pure buoyancy driven mixing. Figure 7d shows a constant mixing width gradient for the pure shear driven mixing. For the compound KH+RT 1 case shown in Figure 7b, transition from the shear dominated flow to the buoyancy dominated flow is observed around 70-100 cm downstream distance, which corresponds to a Richardson number range of -1.6 to -2.5. The transition is further delayed for the KH+RT 2 case of Figure 7c, due to stronger shear, to a downstream distance of 150-170 cm, which corresponds to a Richardson number range of -1.5 to -1.8. Thus, the transition Richardson number for KH+RT flows at the Atwood number of 0.035 is found to be in the range of -1.5 to -2.5. To further check this result, another experiment with ΔU =0.3 m/s is performed at the same Atwood number and the transition Richardson number found to be closer to -1.5. According to equation (2), at a set Atwood number, the Richardson number is only dependent upon the ratio of $h/(\Delta U)^2$, and this ratio value is in between 4.5-7.0 in the transition region. Thus it can be interpreted that, for KH+RT flows at the Atwood number 0.035, if the $h/(\Delta U)^2$ ratio crosses the value of 4.5-7.0, the velocity gradient ΔU is spread over larger distance across the region, and the rollup structure of the shear cannot act against the buoyancy from this point onwards.

We now consider the Reynolds numbers (Re) obtained in the present KH+RT experiments.. Snider and Andrews [32] defined the mixing layer Reynolds number as $\mathrm{Re}=\dfrac{2hv'}{\upsilon}$ for RTI flows. In this definition, the vertical velocity rms fluctuation v' is calculated based on the assumption that the loss in potential energy is converted into turbulent kinetic energy with linear density profile across the mixing layer. Then the definition for Reynolds number becomes,

$$(12) \qquad \mathrm{Re}=\frac{2h^{\frac{3}{2}}}{\nu}\sqrt{\frac{gA_t}{3}}$$

Under this definition the KH+RT 1 experiment achieved a Reynolds number around 6000 at the end of the channel, and the transition Reynolds number between KHI dominated mixing to RTI dominated mixing is around 800-2000.

B. S3WCA Results

The S3WCA technique, described in the diagnostics section above, is used to measure the instantaneous density and velocity at different points in the channel. Measurements at different streamwise locations from the splitter plate are presented here for the RT, KH+RT 1, KH+RT 2, and KH cases. The vertical velocity mean square fluctuation v' is an important turbulence parameter that governs the mixing width [37], and is measured at the mixing layer centerline. Equation (13) defines v', where v is the vertical velocity measured at an instant, $\bar{v}$ is the mean vertical velocity, and N is the number of samples. According to [34] v' can be related to mixing width growth rate in a self-similar regime by the relation given in equation (14). This equation is derived by differentiating the equation (10) with respect to time $'t'$ from the onset of instability. An interpretation of v' is that it quantifies the fluid movement in the vertical direction that contributes to mixing layer growth. The faster the fluid moves in the vertical direction, the higher the value of v', which indicates faster mixing layer growth. For example, v' increases linearly (Figure 8a) with time (streamwise distance for the present facility) in the RT case, indicating faster moving bubble and spike structures developing with time, thus contributing to the parabolic nature of the mixing layer. Furthermore, if v' remains constant with time for a self-similar plane mixing layer then the mixing layer grows linearly.

$$(13) \quad v' = \sqrt{\sum_N \frac{(v-\bar{v})^2}{N}}$$

$$(14) \quad v' = \frac{dh}{dt} = 2\alpha A_t g t$$
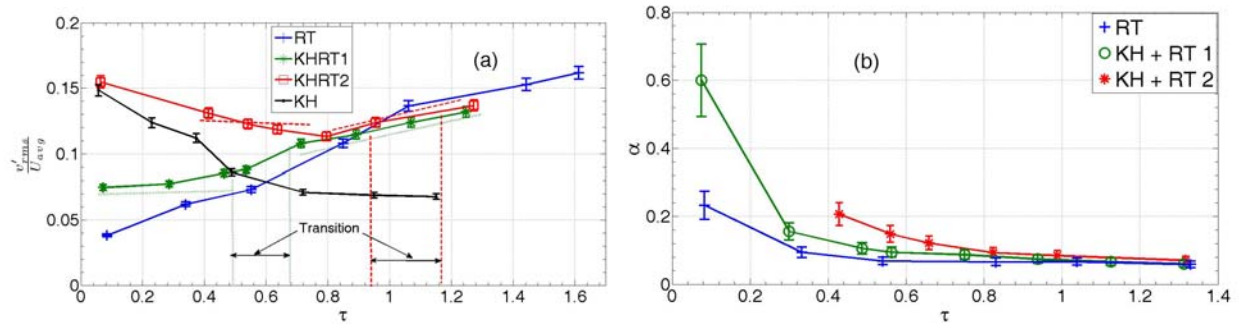
Figure 8: (Color online) (a) Variation of v' along the channel for different cases, (b) Variation of mixing growth coefficient α along the channel calculated from equation (14).

Figure 8 shows the variation of v' along the channel and the growth rate values calculated from equation (14). For the plane mixing layer problem (KH case), the v' value is higher closer to the plate and becomes constant in the self-similar regime. This behavior is similar to the behavior reported by Bell and Mehta [13] for untripped plane mixing layers. This higher value of turbulent normal stress closer to the splitter plate was attributed to larger turbulence production due to higher gradient of streamwise velocity in the boundary layers at the splitter plate compared to tripped initial conditions. For the RT case, v' varies linearly in the self-similar regime. For the KH+RT 1 case, the behavior closer to the splitter plate resembles the KH case, and the linear variation corresponding to RT is observed at the end of the channel. The transition from KH to RT takes place at a location of 60 to 100 cm ($0.45 < \tau < 0.65$) from

the splitter plate, corresponding to a Richardson number of -1.6 to -2.5. Similar transition behavior for KH+RT 2 case is observed at 150-170 cm ($0.95 < \tau < 1.15$) away from splitter plate corresponding to Ri number of -1.5 to -1.8. The length of the present channel is not long enough to observe the transition behavior for KH+RT 3 case. The observations made here support the image analysis results. The growth rate coefficient α value (Figure 8b) is higher closer to the splitter plate for all cases, and it has the highest value for the KH+RT 2 case, which indicates the stronger effect of shear as shown by visualization experiments. The growth rate coefficient for all cases seems to converge to a value between 0.06-0.07 at the end of the channel. All the cases presented in the Figure 8 transitioned to RTI behavior at late time, thus the α values calculated from the Equation (**14**) are valid at late times.

C. Molecular mixing parameter (θ)

Danckwerts [45] quantified the amount of molecular mixing between two different materials by the intensity of segregation (1-θ). The parameter θ is defined by equation (15) below and was first adapted to RTI flows by Youngs [46], and subsequently used by others ([37, 38]) to quantify molecular mixing. Inside the mixing layer, the θ value is equal to 1 when both the fluids are completely molecularly mixed, and θ becomes zero when two fluids are immiscible. In equation (15), ρ is the instantaneous density at a location, whereas $\overline{\rho}$ is the time-averaged density for a total measurement duration of T. The instantaneous density values are obtained from the SW3CA technique. The top stream volume fraction f_1 is defined by (15), where ρ is the measured instantaneous density and ρ_2 is the bottom stream fluid density. The parameter B_0 is the non-dimensional auto correlation of the density, and B_2 is the same correlation for immiscible fluids. In the equation (15), $\overline{f_1}$ is the time averaged top stream volume fraction, and $\overline{f_2}$ is the time averaged bottom stream volume fraction. The value of B_2 is typically close to its maximum of 0.25 at the mixing layer center line for RTI mixing, as equal amounts of molecularly mixed top stream and bottom stream fluids are observed. B_0 measures the rms density fluctuation, and becomes equal to zero either when the fluids are completely mixed, or at the edge of the mix where only one fluid is available.

$$\theta = 1 - \frac{B_0}{B_2}$$

(15)
$$B_0 = \lim_{T \to \infty} \frac{1}{T} \int_0^T \frac{(\rho - \overline{\rho})^2}{(\Delta \rho)^2} \, dt; B_2 = \overline{f_1} \overline{f_2}$$

$$\overline{f_1} = \frac{1}{T} \int_0^T \frac{(\rho - \rho_2)}{\Delta \rho} \, dt; \overline{f_2} = 1 - \overline{f_1}$$

Another parameter Ξ, known as chemical product thickness, defined by equation (16), is also used by many researchers ([47, 48]) to quantify molecular mixing in a fast-kinetic chemical reaction where the product formed is limited by the amount of lean reactant. The definition of Ξ, used by Cook and Dimotakis [47] and Youngs[48], is an integrated parameter across the mixing layer. In the present work another parameter ξ is defined at the centerline of the mixing layer, which is similar to the

parameter Ξ. Banerjee *et al.* [38] have found that the variation of ξ is small across the mixing layer, thus it can be expected that the value of ξ will be close to the value of Ξ. We found that the variation of ξ is identical to the variation of θ along the mixing layer, so either of the parameters can be used to quantify the molecular mixing.

(16)
$$\Xi = \frac{\iint \min(f_1, f_2) dt dy}{\int \min(\overline{f_1}, \overline{f_2}) dy}$$

$$\xi = \frac{\int \min(f_1, f_2) dt}{\min(\overline{f_1}, \overline{f_2})}$$

The variation of θ, measured at the mixing layer centerline, with non-dimensional time $\tau = \frac{x}{U}\sqrt{\frac{A_t g}{H}}$ for RT, KH+RT 1, and KH+RT 2 cases is plotted in Figure 9c. In the late self-similar regime ($\tau > 1$), θ value lies in between 0.72-0.74 for RTI and in good agreement with the previously reported values [37, 38]. At $\tau = 0.83$, where the RT plume structures are smaller in size, the value of θ is less than 0.7. At $\tau = 1.4$, the value of θ is around 0.73 indicating that the fluids are well mixed compared with early times. This higher value of θ at late times is due to large secondary KH rollup structures developed between the bubbles and spikes, creating more interfacial area between the fluids [38].
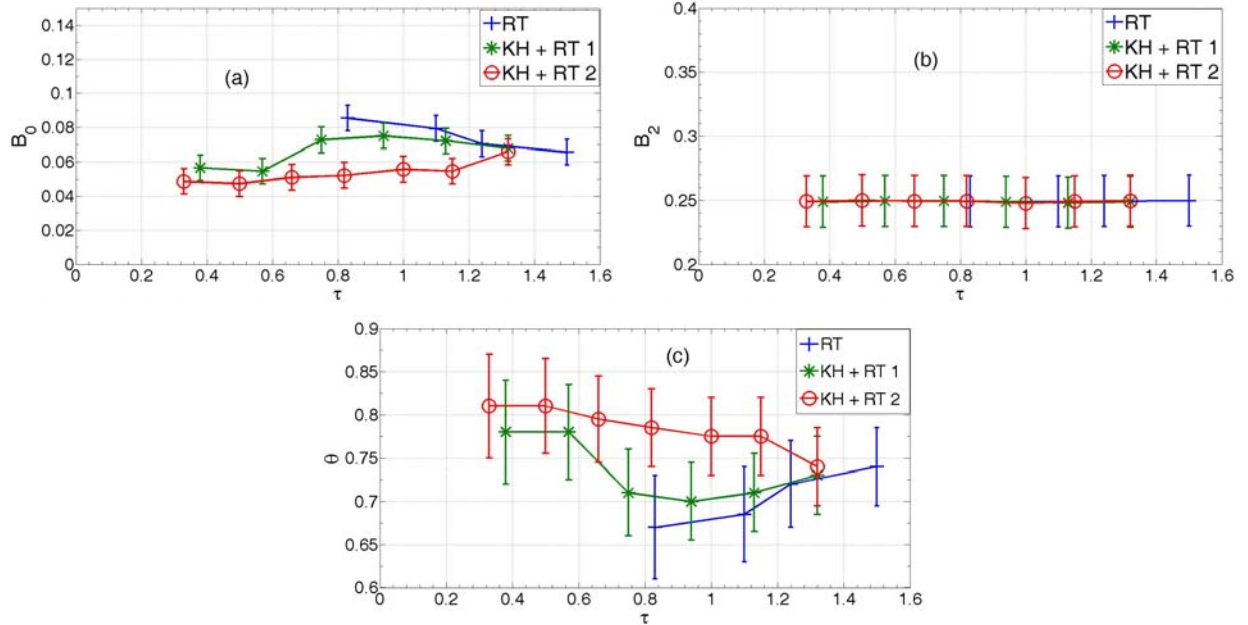
Figure 9: (Color online) Variation of (a) B_0, (b) B_2, and (c) θ with non-dimensional time $\tau = \frac{x}{U}\sqrt{\frac{A_t g}{H}}$ for RT, KH+RT 1 and KH+RT 2 cases respectively.

For KH+RT cases, the molecular mixing is higher at earlier times as indicated by higher values of θ from Figure 9c. For KHI, the mixing layer is dominated by spanwise vortical structures, and these structures create a higher contact area between the two streams compared with RTI structures due to the rolling up of one fluid around another. The larger contact area gives a higher amount of molecular mixing. RTI plume structures are primarily vertical and fine scale mixing is due to shear generated by the rising bubbles and falling spikes. Inspection of Figure 3 shows that the flow is initially dominated by spanwise vortical rollups for the KH+RT cases. For the KH+RT 2 case, θ value is 0.81 at τ=0.3-0.6, and it is higher than the θ value of the self-similar RTI layer. This early time θ value is around 0.78 for the KH+RT 1 case, which is smaller than KH+RT 2 case due to smaller spanwise vortices formed because of the smaller amount of shear. The transition from KHI to RTI happens between τ values of 0.97-1.2 for the KH+RT 2 case, and between 0.4 - 0.6 for the KH+RT 1 case. For both KH+RT cases, before the transition, the θ value is reasonably constant and starts dropping in the transition region. This drop in the value of θ can be attributed to breakup of the rollup structure. The value of θ follows the RTI trend after the transition region, indicated by the values measured at the end of the test section that are close to the RTI values for the KH+RT 1 case. The parameters that define θ, B_0 and B_2 are plotted in Figure 9a,b. The value of B_2 is equal to 0.25 at the center of the mixing layer and the variation B_0 directly affects the variation of θ. A larger value of B_0 (variance of density fluctuation) at the mixing layer centerline shows that the diffusion between the gases is not complete, due to smaller interfacial area in the present case, which gives the smaller value for θ. The variation of B_0 with τ is similar to (mirror) θ as B_2 remained the same for all cases. The probability density function (pdf) distributions of density fluctuations for RT, KH+RT 1, and KH+RT 2 cases are shown in Figure 10. The KH case is not considered here as there is no density difference between the streams.
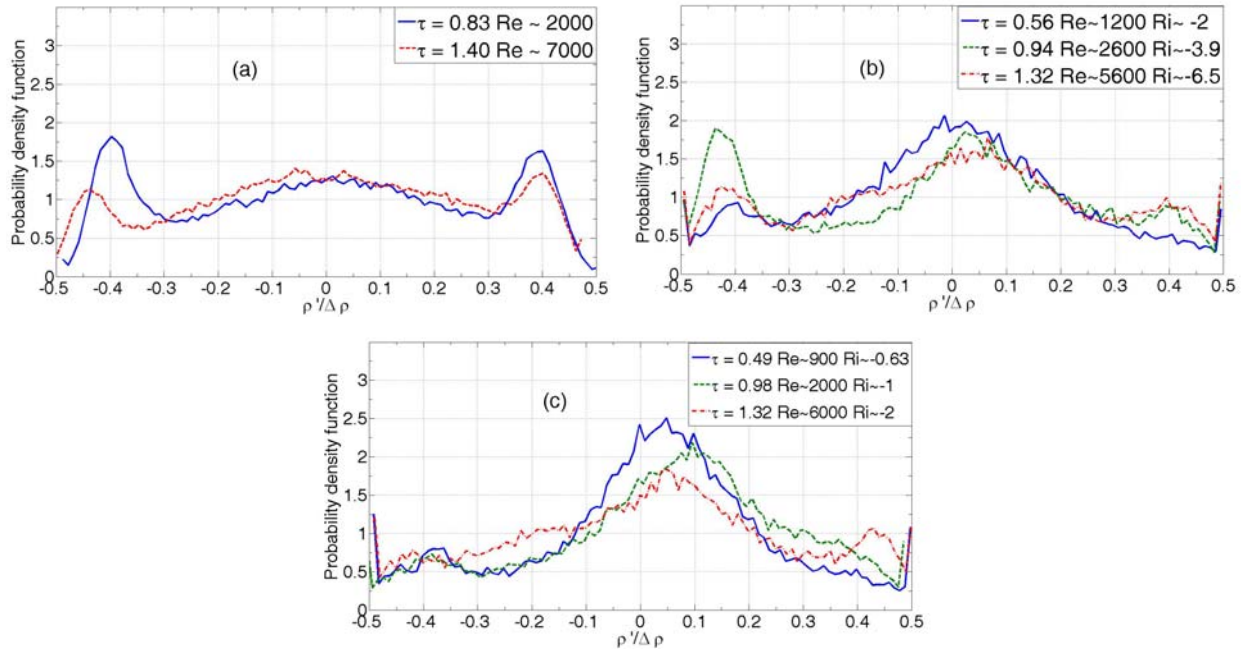
Figure 10: (Color online) Probability density function distribution of density fluctuations at different times $(\tau = \dfrac{x}{U}\sqrt{\dfrac{A_t g}{H}})$ indicated on plots for (a) RT, (b) KH+RT 1, and (c) KH+RT 2.

PDF distribution of density fluctuation is a useful tool to understand the mixing process. The amplitude of the peaks in the PDF distribution and their location on the density fluctuation axis gives information about the amount of fluid present in a particular mixed state as well as the information about that mixing state (whether it is a pure or mixed fluid). For RTI at $\tau = 0.83$, the PDF function in Figure 10a shows two peaks at the ends indicating that a lesser amount of molecularly mixed fluid is available at the center of the mix, which gives a θ value of less than 0.7. Figure 10a also shows a broader and higher peak at the center of the PDF at $\tau =1.4$, indicating that the fluids are well mixed compared with earlier times resulting in higher value of θ (see Figure 9). At early times ($\tau <0.6$) for KH+RT cases, PDF distributions from Figure 10 b,c show a larger peak at the center in contrast to RTI at early times where the distribution is bimodal at the ends with smaller and broader distribution at the center. A higher amount of molecularly mixed fluid is observed at the center of the distribution due to the rollup structure of the KH instability for KH+RT cases at early times. This height of the peak at the center of the PDF for the KHRT2 case is larger (around 2.5 at $\tau = 0.49$) than the late time RTI peak height at the center (around 1.5 at $\tau =1.4$). This shows that the primary rollup structure of shear is more effective in molecularly mixing the fluids than the vertical plume structure of the RTI where the rollups are small, and higher in numbers. At early times, the KH+RT cases have not shown any peaks at the end of PDF distribution indicating that all the fluid is molecularly mixed with no or little amount of pure fluid. For comparison, the PDF distributions are plotted again in Figure 11 a,b at approximately same τ for all cases. The height of these center peaks is larger for KH+RT2 case compared with the KH+RT1 case at same $\tau \sim 0.95$ (Figure 11a), indicating that the higher amount of shear caused higher amount of molecularly mixed fluid.
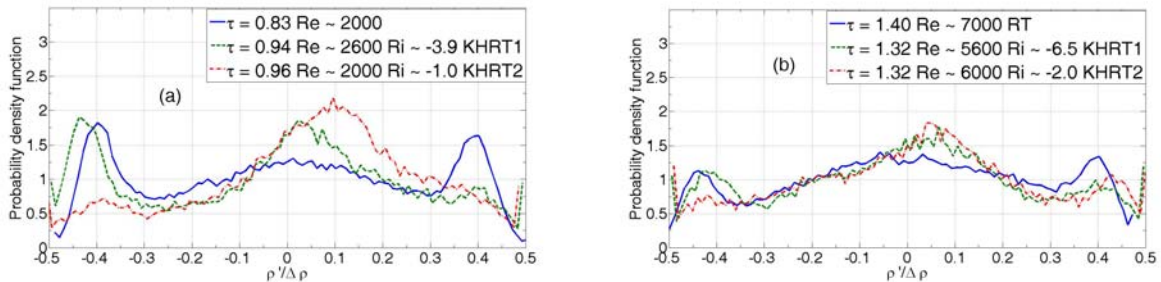
Figure 11: (Color online) Comparison of pdf distributions (from Figure 10) for all the cases at similar values of (a) $\tau \sim 0.9$ (b) $\tau \sim 1.35$.

For KH+RT flows, the amplitude of the peaks at the center of the PDF distributions decreased as the transition region to RTI is approached (Figure 10c, $\tau = 0.98$). The difference between the heights of the center peaks also reduced as both the KH+RT1 and KH+RT2 cases approached transition to RTI (Figure 11b). As the rollup structure has grown in size due to the stretching by buoyancy, and the fresh fluid is entrained into the mixing layer, the amount of fully molecularly mixed fluid present at the center is reduced. However, the θ value in this region is still higher than the self-similar RTI value. After the transition region, increasingly more fluid is entrained from the free stream, and the rollup structure is

replaced with the RTI vertical plume structure and causes the PDF distribution to look like RTI pdf distributions at late times (Figure 10a τ = 1.4 and Figure 10b τ = 1.32).

V. Conclusions

The effect of shear on Rayleigh-Taylor instability is studied at an Atwood number of approximately 0.035 in a convective-type statistically steady gas channel facility at Texas A&M University. The top stream velocity is varied from 1.0 to 2.0 times that of the bottom stream. Mixing width data obtained from the visualization experiments have shown that the flow closer to the splitter plate is governed by spanwise vortical structures from the Kelvin-Helmholtz instability, while away from the splitter plate it is governed by vertical plume structures from the Rayleigh-Taylor instability. This fact is also confirmed by simultaneous 3 wire and cold wire anemometry used for density and velocity measurements. The growth rate coefficient, calculated based on the vertical velocity fluctuation, appears to converge to a single value (0.06-0.07), which is closer to that of the RT case at the end of the channel, irrespective of the amount of shear present in the flow at the splitter plate. Results from the measurements suggest that a transition from KHI-like behavior to RTI-like behavior for compound shear and buoyancy driven flows occurs around a Richardson number value of -1.5 to -2.5 at the Atwood number of 0.035. PDF distributions of density fluctuations, and the molecular mixing parameter θ, for different cases at the mixing centerline indicate that the rollup structure of KHI is more effective in molecularly mixing the fluids at the mixing layer center line than the RTI plume structure where the rollup structure is small (secondary) and higher in numbers. This observation has significant implications for reactive flows.

References

[1]   J. S. Turner, Buoyancy effects in fluids, Cambridge Univ Pr, 1980.
[2]   K. Nagata and S. Komori, J. Fluid Mech. **408**, 39 (2000).
[3]   J. Imberger and P. Hamblin, Annu. Rev. Fluid Mech. **14**, 153 (1982).
[4]   D. H. Sharp, Physica D **12**, 3 (1984).
[5]   S. Chandrasekhar, Hydrodynamic and hydromagnetic stability, Dover Pubns, 1961.
[6]   K. O. Mikaelian, Phys. Fluids **6**, 1943 (1994).
[7]   N. M. Hoffman, M. Hooper, and P. Osborne, Laser Plasma Interactions 5: Inertial Confinement Fusion, 105 (1994).
[8]   V. Thomas and R. Kares, Phys. Rev. Lett. **109**, 75004 (2012).
[9]   D. L. Youngs, Physica D **12**, 32 (1984).
[10]   P. G. Drazin and W. H. Reid, Hydrodynamic stability, Cambridge Univ Pr, 2004.
[11]   D. Lewis, Proceedings of the Royal Society of London. Series A, Mathematical and Physical Sciences, 81 (1950).
[12]   K. Read, Physica D **12**, 45 (1984).
[13]   J. H. Bell and R. D. Mehta, AIAA Journal **28**, 2034 (1990).
[14]   S. B. Pope, Turbulent flows, Cambridge Univ Pr, 2000.
[15]   G. Dimonte, D. Youngs, A. Dimits, S. Weber, M. Marinak, S. Wunsch, C. Garasi, A. Robinson, M. Andrews, and P. Ramaprabhu, Phys. Fluids **16**, 1668 (2004).

[16]   H. Görtler, ZAMM - Journal of Applied Mathematics and Mechanics / Zeitschrift für Angewandte Mathematik und Mechanik **22**, 244 (1942).
[17]   C. M. Sabin, J. Basic Engg. **87**, 421 (1965).
[18]   H. W. Liepmann and J. Laufer, NACA TN **1257**, (1947).
[19]   A. Yule, ARC R & M **3683**, (1971).
[20]   C. Winant and F. Browand, J. Fluid Mech. **63**, 237 (1974).
[21]   F. Browand and P. Weidman, J. Fluid Mech. **76**, 127 (1976).
[22]   G. L. Brown and A. Roshko, J. Fluid Mech. **64**, 775 (1974).
[23]   M. Koochesfahani and P. Dimotakis, J. Fluid Mech. **170**, 83 (1986).
[24]   J. Lasheras and H. Choi, J. Fluid Mech. **189**, 53 (1988).
[25]   S. Thorpe, J. Fluid Mech. **32**, 693 (1968).
[26]   S. Thorpe, Boundary Layer Meteorol. **5**, 95 (1973).
[27]   S. Thorpe, J. Fluid Mech. **61**, 731 (1973).
[28]   F. Browand and C. Winant, Boundary Layer Meteorol. **5**, 67 (1973).
[29]   C. Koop and F. Browand, J. Fluid Mech. **93**, 135 (1979).
[30]   U. Shumlak and N. Roderick, Phys. Plasmas **5**, 2384 (1998).
[31]   D. Snider and M. Andrews, J. Fluids Eng. **118**, 55 (1996).
[32]   D. M. Snider and M. J. Andrews, Phys. Fluids **6**, 3324 (1994).
[33]   G. Lawrence, F. Browand, and L. Redekopp, Phys. Fluids A **3**, 2360 (1991).
[34]   D. Snider and M. Andrews, J. Fluids Eng. **118**, 370 (1996).
[35]   B. J. Olson, J. Larsson, S. K. Lele, and A. W. Cook, Phys. Fluids **23**, 114107 (2011).
[36]   A. Banerjee and M. J. Andrews, Phys. Fluids **18**, 035107 (2006).
[37]   P. Ramaprabhu and M. Andrews, J. Fluid Mech. **502**, 233 (2004).
[38]   A. Banerjee, W. N. Kraft, and M. J. Andrews, J. Fluid Mech. **659**, 127 (2010).
[39]   W. N. Kraft, Dissertation submitted to Texas A&M University, (2008).
[40]   W. N. Kraft, A. Banerjee, and M. J. Andrews, Exp. Fluids **47**, 49 (2009).
[41]   M. Richmond, Newyork, p. http://spiff.rit.edu/classes/phys440/lectures/optd/optd.html, 2003.
[42]   M. Hishida and Y. Nagano, J. Heat Transfer **100**, 340 (1978).
[43]   P. V. Vukoslavčević, I. M. Radulović, and J. M. Wallace, Exp. Fluids **39**, 703 (2005).
[44]   J. A. Zufiria, Phys. Fluids **31**, 440 (1988).
[45]   P. Danckwerts, Appl. Sci. Res. **3**, 279 (1952).
[46]   D. L. Youngs, Phys. Fluids A **3**, 1312 (1991).
[47]   A. W. Cook and P. E. Dimotakis, J. Fluid Mech. **443**, 69 (2001).
[48]   D. Youngs, in Sixteenth AIAA Computational Fluid Dynamics Conference, Vol. Tech. Rep. no. 4102., 2003.